

In situ polymerized succinonitrile-based solid polymer electrolytes for lithium ion batteries

Kai Liu^{a,b,e}, Qingqing Zhang^a, Bishnu P Thapaliya^{b,e}, Xiaoguang Sun^b, Fei Ding^{c*}, Xingjiang Liu^{a,c}, Jinli Zhang^{a,d*}, Sheng Dai^{b,e}

^a School of Chemical Engineering and Technology, Tianjin University, Tianjin 300350, P. R. China.

^b Chemical Science Division, Oak Ridge National Laboratory, Oak Ridge, TN 37831, USA.

^c National Key Laboratory of Science and Technology on Power Sources, Tianjin Institute of Power Sources, Tianjin 300384, P. R. China.

^d School of Chemical Engineering, Shihezi University, Shihezi 832003, P. R. China.

^e Department of Chemistry, University of Tennessee, Knoxville, TN 37996, USA.

*Corresponding author's email address: feiding_ncps@163.com; zhangjinli@tju.edu.cn

Abstract: Novel solid polymer electrolytes based on succinonitrile (SN) plastic crystal electrolyte (SN-PCE) and polymerized ionic liquid (PIL) has been successfully synthesized *via* an in-situ method. The fabricated electrolyte (PIL-SN-PCE) is uniformly inlaid into the supporting matrix of polyimide, which effectively ameliorates the mechanical properties of the electrolyte. PIL can effectively enhance the thermal stability of electrolytes up to 300 °C and mitigate the parasitic reactions between the electrolytes and the electrodes. PIL-SN-PCE exhibits a remarkable oxidation ability up to 5.4 V vs Li/Li⁺ and a high room temperature ionic conductivity of 6.54×10^{-4} S cm⁻¹. Furthermore, in-situ formed interface in PIL-SN-PCE guarantee an excellent compatibility with different electrodes, which can effectively improve

the cycle stability and rate performances of both half-cells and full cells. Thus, PIL-SN-PCE is considered as a promising electrolyte for high energy density lithium-ion batteries.

Keywords: Succinonitrile; In-situ method; Polymerized ionic liquid; Lithium-ion batteries

1. Introduction

Lithium ion batteries (LIBs) are crucial in the current cutting-edge energy storage devices with expeditious development of sophisticated portable electronic devices, hybrid-electric vehicles, and electric vehicles [1-5]. However, conventional LIBs based on liquid electrolyte still confronts with a series of safety issues such as the leakage and ignition of electrolyte or even explosion [6-8]. To mitigate the aforementioned tricky issues, solid state electrolytes (SSEs) have been extensively investigated due to their extraordinary safety characteristics and excellent interface compatibility toward metal lithium, which has shown tremendous potential as anode of lithium metal batteries to drive electric vehicles in the future [9-10]. Generally, SSEs can be divided into two types, namely inorganic electrolytes and polymer electrolytes [11-15]. Inorganic garnet-type electrolytes usually exhibit a high ionic conductivity comparable to that of liquid electrolytes and have a high elastic modulus to prevent the growth of lithium dendrite. However, its inherent brittleness and inferior interphase compatibility with cathodes have hampered their further application [16-17]. Although sulfide-based electrolytes can overcome those limitations of garnet-based electrolytes, the preparation environment is extremely rigorous with the content of H₂O and O₂ less than 0.1 ppm [18-19]. Compared with

inorganic electrolytes, solid polymer electrolytes have better interphase compatibility with the cathodes because of their intrinsic flexibility [20]. The widely common polymer matrix are mainly centered at the poly(methyl methacrylate) (PMMA) [21], poly(vinylidene fluoride) (PVDF) [22], polyacrylonitrile (PAN) [23], poly(ethylene oxide) (PEO) [24] and so on. Unfortunately, low room temperature ionic conductivities, limited electrochemical window and inflammable nature have restricted their wide application in LIBs.

Recently, plastic crystal electrolyte (PCE) prepared by dissolving lithium salts into plastic crystals has been extensively investigated due to its solidity in wide temperature range and higher ambient solid state ionic conductivity [25-28]. It presents the unique properties of long-range position order with orientational disorder. Succinonitrile (SN) as a typical representative displays the classic plastic crystal characteristics within the temperature range from -40 °C to 60 °C. The SN based PCE (SN-PCE) shows negligible vapor pressure, low flammability, wide electrochemical window and fast ion-conductivity up to 10^{-3} S cm⁻¹ at 25 °C [29-30]. Unfortunately, the SN-PCE behaves the liquid-like features and cannot form self-supporting SSE film because of its lacking mechanical strength. To overcome this problem, SN-PCE has been incorporated into the organic polymers by ultraviolet irradiation (UV-curing) or simple mechanical agitation methods [31-35]. However, ultraviolet light is known to be harmful to the health of human body and both methods usually also lead to the poor interfacial compatibility between electrolytes and electrodes. More importantly, these organic polymers usually have low ignition points and inferior thermal stability that could still compromise the safety of LIBs [36-38].

To construct a much safer SSE with high ambient ionic conductivity, high thermal

stability and good interfacial compatibility with electrodes, an ionic liquid has been in-situ thermally polymerized in the presence of SN-PCE (PIL-SN- PCE) on a polyimide supporting matrix. The PIL-SN- PCE shows non-flammable characteristic with a thermal stability up to 300 °C, an ionic conductivity of $6.54 \times 10^{-4} \text{ S cm}^{-1}$ at 25 °C, and an electrochemical window higher than 5.4 V (vs Li/Li⁺). In addition, the half-cell of LiFePO₄/PIL-SN-PCE/Li exhibits a high initial reversible capacity of 156.5 mAh g⁻¹ at 0.1 C with a capacity retention of 93.3% after 70 cycles and retains 66% discharge capacity of cells at charge-discharge current density of 1 C compared with that of its cycling at 0.1 C. Furthermore, the full cell of LiFePO₄/ PIL-SN- PCE/LTO delivers a reversible capacity of 132.4 mAh g⁻¹ at 0.5 C with a capacity retention of 90.3% after 50 cycles.

2. Experimental Section

Succinonitrile (SN), lithium bis-(trifluoromethanesulfonimide) salt (LiTFSI with purity >99.99%) and azobis-isobutyronitrile (AIBN) were purchased from the Sigma-Aldrich company. 1-vinyl-3-methylimidazolium bis[(trifluoromethyl)sulfonyl]imide (VMIMTFSI) was obtained from Lanzhou Institute of Chemical Physics. Polyimide separator (thickness, 30um; porosity, 43%, pore size, 0.045) was supplied by Tianjin Institute of Power Sources.

2.1 Preparation of SN-PCE, PIL-SN- PCE and Solid State Batteries

The SN-PCE was obtained by dissolving lithium bis-(trifluoromethanesulfonimide) salt (LiTFSI) into SN at 60 °C to form 1 M solution inside an argon filled glove box. The ionic liquid of 1-vinyl-3-methylimidazolium bis[(trifluoromethyl)sulfonyl]imide (VMIMTFSI) was dried using 4Å molecular sieves for a week with a final moisture content of 25 ppm. PIL-SN-

PCE was prepared as following: VMIMTFSI was first mixed with SN-PCE in different proportions of 40:60, 45:55, and 50:50 to form a homogeneous solution and denoted as a-PIL-SN-PCE, b-PIL-SN-PCE and c-PIL-SN-PCE, respectively. Thermal initiator of azobisisobutyronitrile (AIBN, 1 wt.%) was then dissolved into the precursor solution in a vial. The as-prepared PIL-SN-PCE precursor was placed in an oven at 70 °C under nitrogen atmosphere for 30 min to complete the polymerization. Solid state 2430 button batteries were fabricated by using PI as the supporting matrix and PIL-SN-PCE precursor as the electrolytes, which was then in-situ polymerized at 70 °C for 30 min. The schematic preparation procedure for the electrolytes was illustrated in **Fig. 1**.

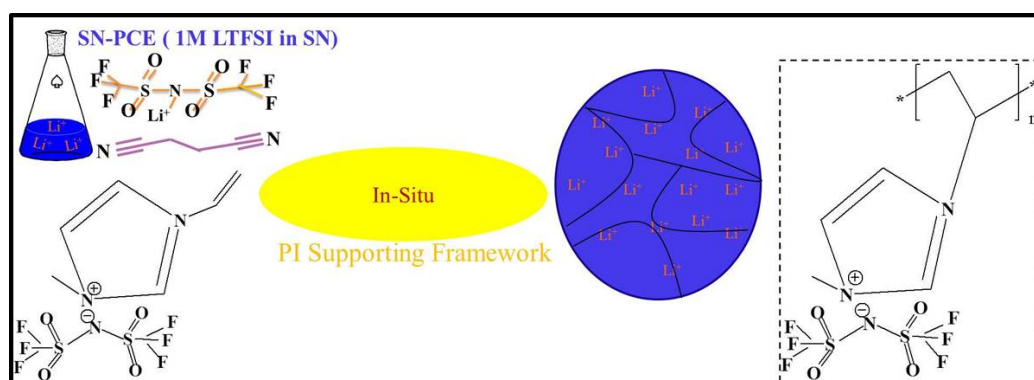


Fig. 1. Scheme of preparation procedure for PIL-SN-PCE electrolytes

2.2 Characterization of PIL-SN-PCE and Solid State Battery

The free-radical thermal curing reaction of SN-PIL-PCE was examined by a FT-IR spectrometer (Nicolet 6700) with a spectral resolution of $<0.09\text{ cm}^{-1}$. The stress-strain curve of polyimide was attained by the universal testing machine (WDW-10) with a force sensor (BAB-10MT) as shown in Fig. S1. Thermogravimetric analysis (TGA) was measured on a Setsys Evolution TG/DSC-16 instrument from 25 °C to 500 °C at a heating rate of 10 °C min^{-1}

under an argon atmosphere and the combustibility experimentation of electrolyte was inspected by using burning cotton balls to ignite it. The cross-section morphologies were investigated by scanning electron microscopy (SEM; Hitachi S-4800). The phase transition temperature of SN, SN-PCE and SN-PIL-PCE were taken on TG-DSC equipment with ramp rates of 5 °C min⁻¹ from -60 °C to 100 °C at a sealed quartz pans under the N₂ conditions. X-ray diffraction (XRD) was performed by using Cu K α radiation ($\lambda = 1.5406 \text{ \AA}$) with the 2 θ range from 10° to 90° at an operation voltage of 40 kV and a current of 40 mA. Ionic conductivity ($\sigma = L * R/A$; R was the impedance value; L and A was the thickness and surface area of electrolytes, respectively) was measured by using electrochemical impedance spectroscopy (EIS) on an Auto-lab PGSTAT 2273 working station over a frequency range from 10⁻² to 10⁻⁶ Hz at the temperature range from 25 °C to 90 °C. The lithium ion transference number (t_{Li^+}) of PIL-SN-PCE electrolyte was tested by a steady-state polarization method on the symmetric Li/PIL-SN-PCE/Li cell. The polarization current curve (I^0 and I^{ss} stands for the initial and steady state current value, respectively) was recorded by putting a constant polarization potential ($\Delta V = 5 \text{ mV}$) on this cell. The before and after polarization values of interface resistances (R_i^0 and R_i^{ss}) and bulk resistance (R_b^0 and R_b^{ss}) were estimated by EIS measurement. The t_{Li^+} can be calculated by the equation: $t_{Li^+} = I^{ss} R_b^{ss} (\Delta V - I^0 R_i^0) / I^0 R_b^0 (\Delta V - I^{ss} R_i^{ss})$. The electrochemical stability window of PIL-SN-PCE was measured by linear sweep voltammetry (LSV) with stainless-steel as working electrode and lithium foils as both counter and reference at a scan rate of 1 mV s⁻¹. The interfacial stability of PIL-SN-PCE towards lithium metal electrodes was evaluated by measuring the time evolution of EIS on a symmetrical Li cell (Li/PIL-SN-PCE/Li) at room temperature over a frequency range from 10⁻² to 10⁶ Hz. Coin cells of CR2430 were

assembled by sandwiching the PIL-SN-PCE between LiFePO_4 cathode ($\text{LiFePO}_4/\text{Super P/PVDF}=8:1:1$, w/w/w) and lithium metal or $\text{Li}_4\text{Ti}_5\text{O}_{12}$ (LTO/Super P/PVDF=8:1:1, w/w/w) anode in an argon filled glove box. The active material loading on cathode and anode is about 2.5 mg cm^{-2} and 2.8 mg cm^{-2} , respectively. The cycle performance of half and full cell with the voltage range from 2.5 V to 4.2 V is obtained on the LAND CT-2001 battery testing instrument (Wuhan, China) at the current densities of $0.0425 \text{ mA cm}^{-2}$ and $0.2125 \text{ mA cm}^{-2}$, respectively. The rate performances of half cells were performed at different current densities ($1 \text{ C}=170 \text{ mA g}^{-1}$) in the voltage range of 2.5 and 4.2 V vs. Li/Li^+ .

3. Results and Discussion

The cross-section SEM of pristine PI and PIL-SN-PCE electrolyte embedded in the PI supporting framework are presented in Fig. 2(a)-(d). One apparent trend is that the supporting framework textures become denser and compact with more PIL-SN-PCE presence, particularly the sample of c-PIL-SN-PCE in Fig. 2(d). The successful polymerization of precursors at $70 \text{ }^\circ\text{C}$ for 30 min is demonstrated in the insets of Fig. 2(b)-(d) for different composition precursors of PIL-SN-PCE sealed in a small vial. The yellow and jelly-like quasi-solid electrolyte can effectively fasten the white magnetic stir bar when the vial is inverted, indicating these electrolytes are not free-flowing. Meanwhile, the optical photographs and whole cross-section images of pristine PI and PIL-SN-PCE are also displayed in Fig. S2 and Fig. S3, respectively. The solidity of the electrolyte can effectively ameliorate the leakage issue of conventional organic liquid electrolyte, which usually causes safety problems of LIBs.

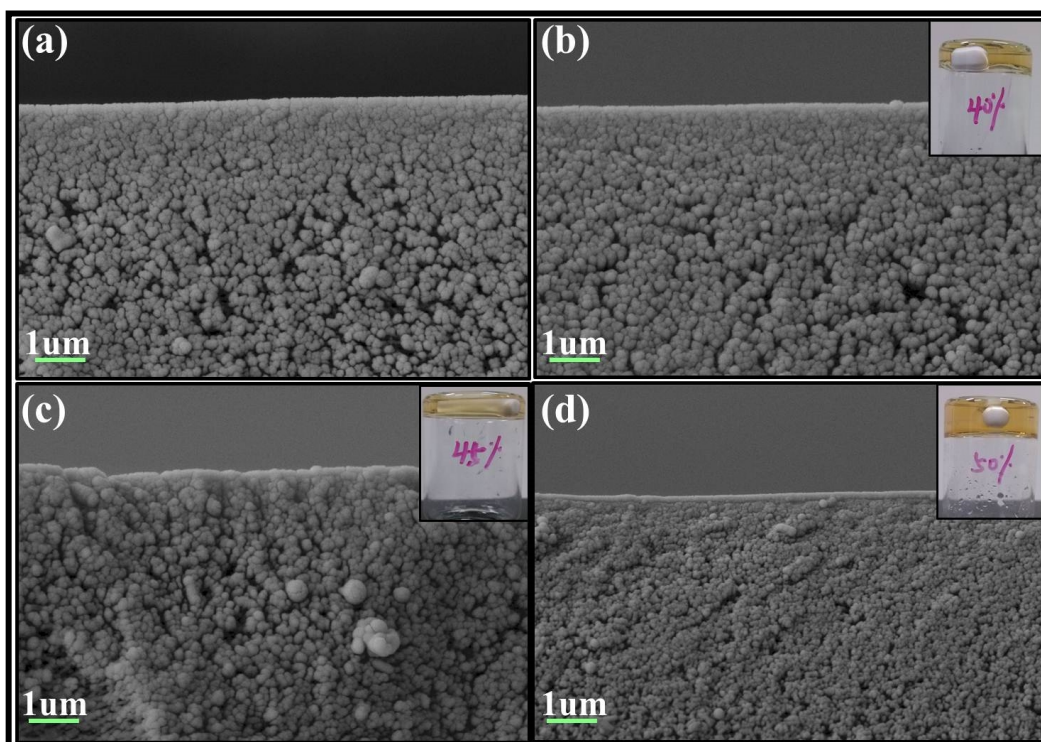


Fig. 2. Cross-section morphological characteristics of pristine PI (a), polymerized PIL-SN-PCE electrolyte embedded into the PI supporting framework (b) a-PIL-SN-PCE, (c) b-PIL-SN-PCE, and (d) c-PIL-SN-PCE as well as the inserted optical images of a-PIL-SN-PCE (b), b-PIL-SN-PCE (c), c-PIL-SN-PCE (d).

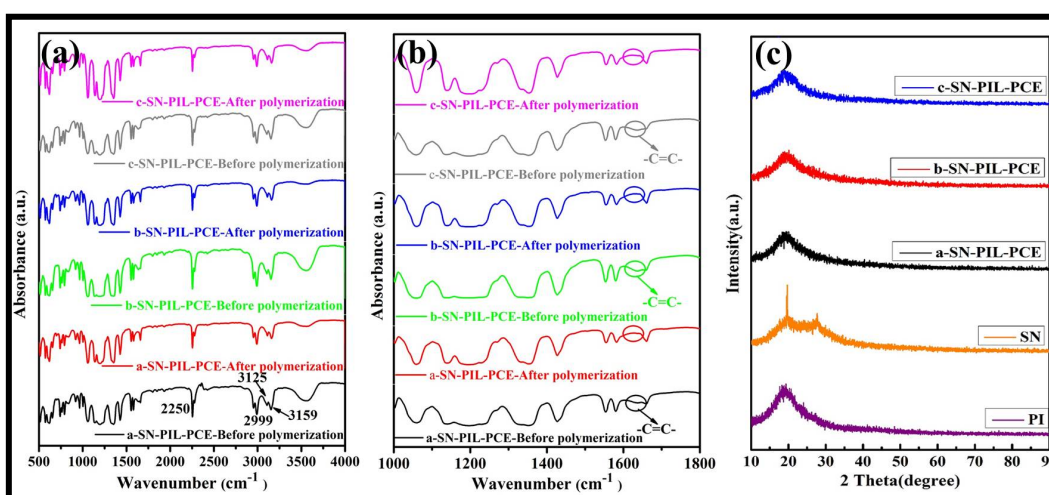


Fig. 3. FTIR spectrum of a-SN-PIL-PCE, b-SN-PIL-PCE and c-SN-PIL-PCE before/after polymerizing (a), (b) Their part magnification; (c) XRD pattern of PI coating film, pure SN, a-SN-PIL-PCE, b-SN-PIL-PCE and c-SN-PIL-PCE after polymerizing.

In order to expound the polymerization reaction mechanism of SN-PIL-PCE, FT-IR spectrometer is used as can be seen in Fig. 3(a)-(b). The characteristic peaks of 2250 cm^{-1} and 2999 cm^{-1} are ascribed to the gauche-trans stretching of $\text{C}\equiv\text{N}$ and CH for SN and the peaks approximately to 3125 cm^{-1} and 3159 cm^{-1} are originated from the CH₂ and CH₃ of VMIMTFSI as displayed in Fig. 3(a), which is similar with the previous reported literatures [39-40]. The appearance of these feature peaks imply SN has been compounded with VMIMTFSI uniformly. In addition, the peak related to the C=C double bonds before polymerizing emerges in the precursor of SN-PIL-PCE as shown in Fig. 3(b). However, this characteristic peak is disappeared after thermal curing for 30 min at $70\text{ }^{\circ}\text{C}$, which demonstrates the precursor has been polymerized consistent with the result of Fig. 2. The evolution of different materials crystallinity is evaluated by means of XRD pattern in Fig. 3(c). In order to avoid exposing materials to air, all samples are coated by PI film. As shown in Fig. 3(c), pure PI coating film displays a similar shape with bread diffraction peak at 19.5° . However, the experiment outcome derived from PI-coated SN exhibits two high crystal degree peaks at about 19.5° and 28.2° respectively. SN-PIL-PCE with different constitutions after polymerizing at $70\text{ }^{\circ}\text{C}$ behaves a lower crystallinity approximating to the amorphous state comparing with pure SN. This feature is mainly ascribed to the interactions among the Li^+ , nitrile functional groups and ionic liquid, increasing the lattice defect (trans-isomers) concentrations in SN, which improve the room temperature ionic conductivity of electrolytes [41-42]. Therefore, the above results imply this type of electrolytes can be used as a promising electrolyte in the field of LIBs well.

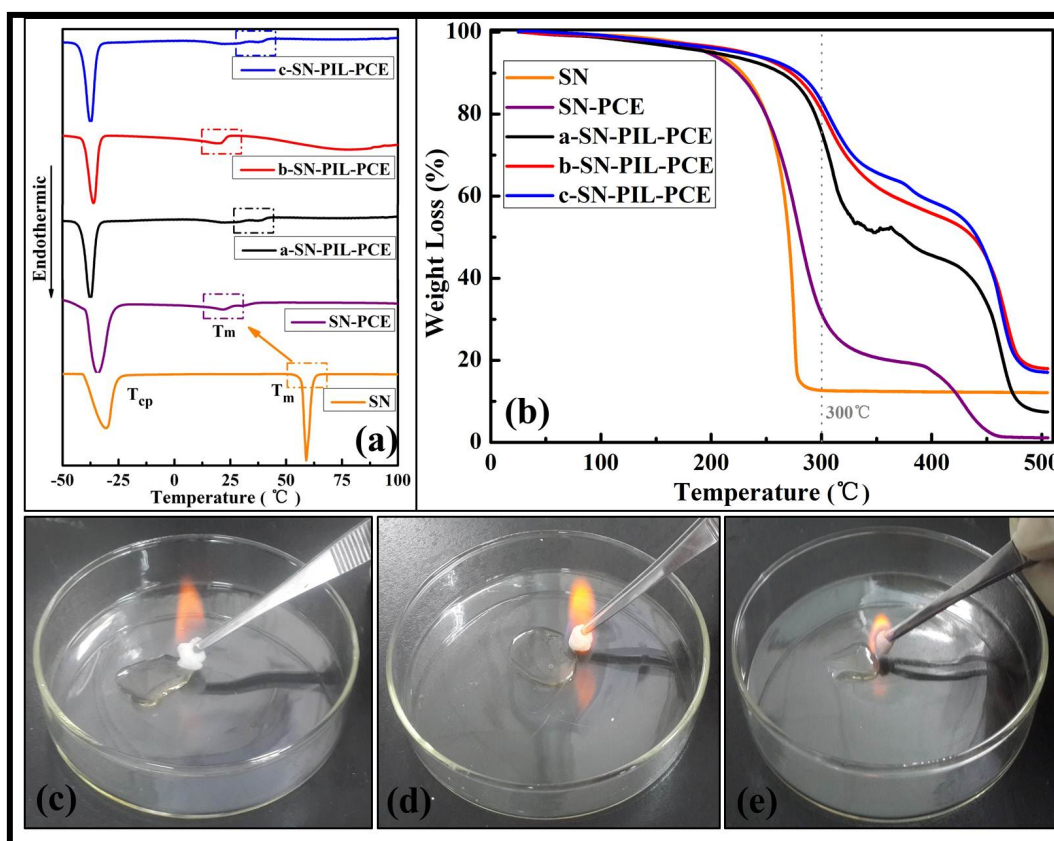


Fig. 4. DSC images (a) and TGA curves (b) of SN, SN-PCE, a-SN-PIL-PCE, b-SN-PIL-PCE and c-SN-PIL-PCE; (c-e) Combustion experiments of a-SN-PIL-PCE, b-SN-PIL-PCE and c-SN-PIL-PCE

The plastic crystal feature of electrolytes is further explored by implementing the TG-DSC experiment. As exhibited in the Fig. 4(a), the pure SN represents two obvious endothermic peaks at $-33.2\text{ }^{\circ}\text{C}$ and $59.3\text{ }^{\circ}\text{C}$, which is corresponded to the phase transition from crystal state to plastic crystal state (T_{cp}) and following to liquid state (T_m), respectively. When LiTFSI integrates into pure SN forming the SN-PCE, the T_{cp} almost has no alternation and the T_m shifts toward left from $59.3\text{ }^{\circ}\text{C}$ to $24\text{ }^{\circ}\text{C}$ with broadening diffraction peak, in which suggests the deterioration of crystal structure for pure SN due to the complexation of difference ionic and the incurrence of high quantity structure defects [43-45]. Accompanied by incorporating of ionic liquid into SN-PCE solution and then through the high temperature heating cure, all SN-PIL-PCE samples show the similar T_{cp} and T_m

with SN-PCE, which indicate thermal features of SN-PCE is not been disturbed. This lower T_m is beneficial to improve the transport of Li^+ . Fig. 4(b) represents the TGA curves of SN, SN-PCE and all PIL-SN-PCE samples. As can be seen from the Fig. 4(b), SN and SN-PCE exhibit similar thermal stability up to 230 °C. As a comparison, the thermal stabilities of PIL-SN-PCEs significantly increase up to 300 °C, suggesting the introduction of VMIMTFSI can effectively improve the safety of the electrolytes. In the meanwhile, the thermo-stability of the electrolyte systematically increases with increasing the amount of VMIMTFSI in PIL-SN-PCE. Table 1 compares the thermostabilities of PIL-SN-PCE with different types of plastic crystal-based electrolytes in the literature. As shown in Table 1, PIL-SN-PCE displays the best thermal stability among these electrolytes [26,32,34,35,42,45-47]. Besides, Fig. 4(c)-(e) shows the combustion experiments of a-SN-PIL-PCE, b-SN-PIL-PCE and c-SN-PIL-PCE. It is can be seen that all SN-PIL-PCE are flame-retardant compared with those of carbonate-based electrolytes, implying this types of electrolytes can significant ameliorate the safety properties of LIBs.

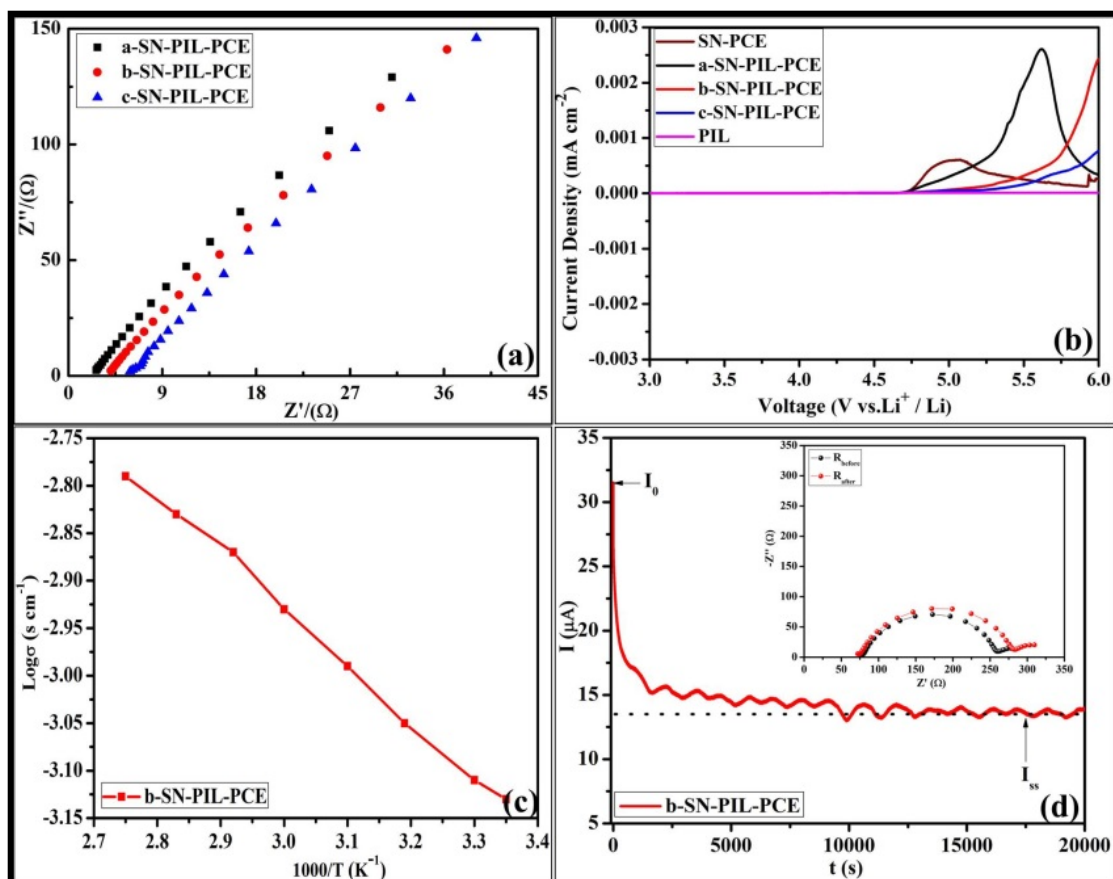


Fig. 5. (a) Electrochemical impedance spectroscopy of a-PIL-SN-PCE, b-PIL-SN-PCE and c-PIL-SN-PCE electrolyte and (b) LSV curves of SN-PCE, a-PIL-SN-PCE, b-PIL-SN-PCE and c-PIL-SN-PCE.

High Li^+ conductivity and wide electrochemical window are crucial for the electrolyte in high energy density LIBs. Fig. 5(a) shows the electrochemical impedance spectroscopy (EIS) of the three samples with different compositions. The resistance increases with increasing the amount of VMIMTFSI. The calculated ionic conductivities of the three samples are listed in Table 2. The highest ionic conductivity of $9.95 \times 10^{-4} \text{ S cm}^{-1}$ is for a-PIL-SN-PCE. Unfortunately, its electrochemical stability window is only up to 4.6 V as show in Fig. 5(b), which is consistent with the stability of SN-PCE. However, the stability window of PIL-SN-PCE systematically increases with increasing the amount of VMIMTFSI, which increases up to 5.6 V for c-PIL-SN-PCE. This is mainly ascribed to high electrochemical window of

VMIMTFSI (above 6V). Based on the thermal stability, ionic conductivity and LSV result, b-PIL-SN-PCE might be the best electrolyte for application in LIBs. Besides, temperature-dependent ionic conductivity of this solid electrolyte also is investigated as shown in the Fig. 5(c). The ionic conductivity of b-PIL-SN-PCE clearly improves accompanying with the rise of temperature. This is mainly ascribed to rapidly migration of lithium ions at high temperature, which is beneficial to enhance the ionic conductivity of b-PIL-SN-PCE. Lithium ion transference number (t_{Li^+}) is another value judgement standard for characteristic of lithium batteries. The t_{Li^+} of b-PIL-SN-PCE is presented in Fig. 5(d) using Li/b-PIL-SN-PCE/Li cell. Comparing with t_{Li^+} of conventional liquid electrolyte (0.38) as previous reported [32], b-PIL-SN-PCE shows an improved t_{Li^+} up to 0.43, which can retard the polarization of batteries during charge-discharge process.

Table 1. Compositions of different samples and property of physical and electrochemical

Sample	Thermal stability	Ionic conductivity	Electrochemical window	Discharge capacity
PET Immersed in (ETPTA/PCE) ^[46]	150°C	$5.7 \times 10^{-4} \text{ S cm}^{-1}$	—	120 mAh g ⁻¹
ETPTA/PCE ^[45]	—	$> 10^{-3} \text{ Scm}^{-1}$	5v	—
TPPTA/PCE ^[45]	—	$> 10^{-3} \text{ Scm}^{-1}$	4.5v	—
ETPTA/PVDF-HFP/PCE ^[42]	—	$> 10^{-3} \text{ Scm}^{-1}$	>5v	92 mAh g ⁻¹
ETPTA/Al ₂ O ₃ /PCE ^[47]	130°C	$1.02 \times 10^{-3} \text{ S cm}^{-1}$	>5v	—
TPPTA/Al ₂ O ₃ /PVDF-HFP/PCE ^[34]	200°C	$1.03 \times 10^{-3} \text{ S cm}^{-1}$	>5.2v	135.1 mAh g ⁻¹
PVA-CN/SN ^[32]	200°C	0.3S	5v	97.7 mAh g ⁻¹
PPS-SPE ^[35]	100°C	$4.0 \times 10^{-4} \text{ S cm}^{-1}$	4.8v	101.6 mAh g ⁻¹
PIL-SN-PCE	300°C	$6.54 \times 10^{-4} \text{ S cm}^{-1}$	>5.4v	105.3 mAh g ⁻¹

Table 2. Conductivity of different samples at 25°C

Sample	VMIMTFSI: SN (w/w)	conductivity (S cm ⁻¹)
a-SN-PIL-PCE	40:60	9.95×10^{-4}
b-SN-PIL-PCE	45:55	6.54×10^{-4}
c-SN-PIL-PCE	50:50	4.49×10^{-4}

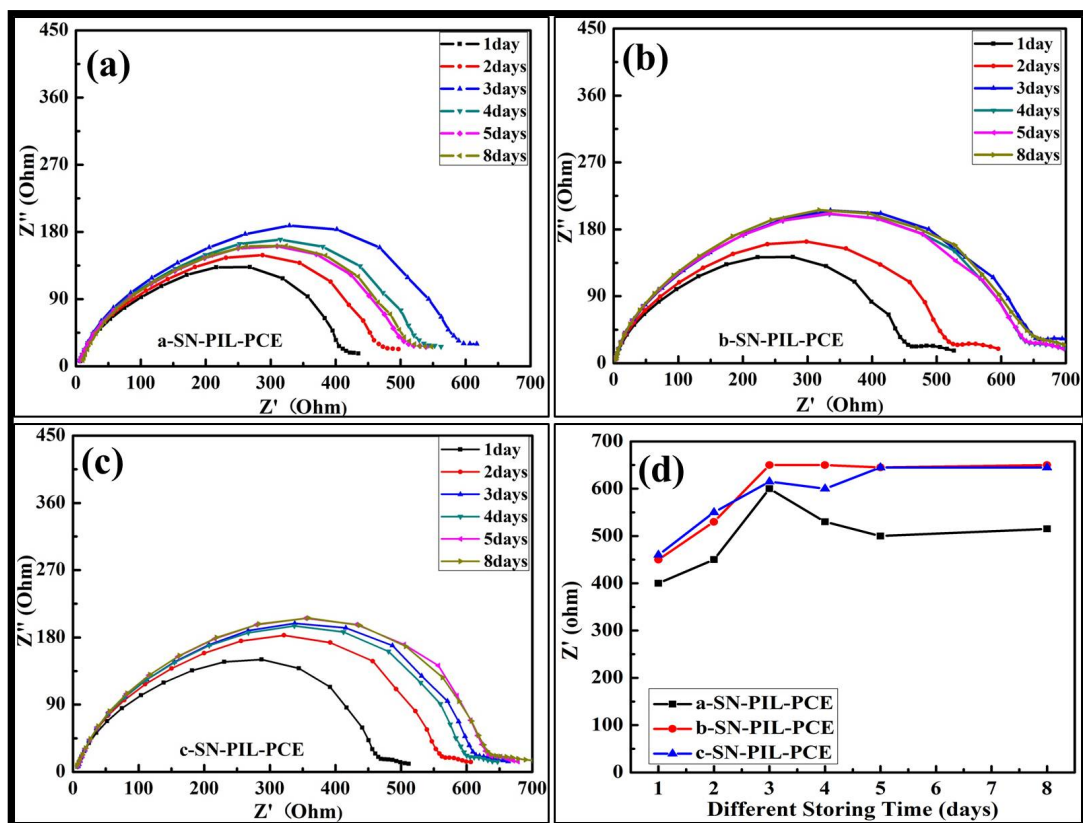


Fig. 6. Evolution of EIS of Li/PIL-SN-PCE/Li symmetrical batteries with different aging time (a) a-PIL-SN-PCE, (b) b-PIL-SN-PCE and (c) c-PIL-SN-PCE; Summary the interfacial impedance value evolutions of a-PIL-SN-PCE, b-PIL-SN-PCE and c-PIL-SN-PCE as time goes on (d).

The interfacial stability of PIL-SN-PCE towards metal lithium is evaluated by the time evolution of EIS of symmetric Li/PIL-SN-PCE/Li cells, as depicted in the Fig. 6. The semicircle in the EIS represents the interfacial resistance between the electrolyte and the lithium electrodes. As can be seen from Fig. 6(a), the interfacial resistance of a-PIL-SN-PCE is unstable with storage time, although its impedance value is relatively low, which is mainly attributed to the side reactions between SN and lithium as previously reported [48-49]. As a comparison, the EIS of b-PIL-SN-PCE gradually rapidly increase with time and then stabilizes after 3 days as shown in Fig. 6(b), indicating a stable interface layer has been formed on the surface of lithium electrodes. Similarly, c-PIL-SN-PCE also forms relatively stable interfacial

impedance as seen from Fig. 6(c). Fig. 6(d) summarizes the time evolution of the EIS of the three samples. The EIS values of b-PIL-SN-PCE and c-PIL-SN-PCE quickly stabilize after 3 days and 5 days, respectively.

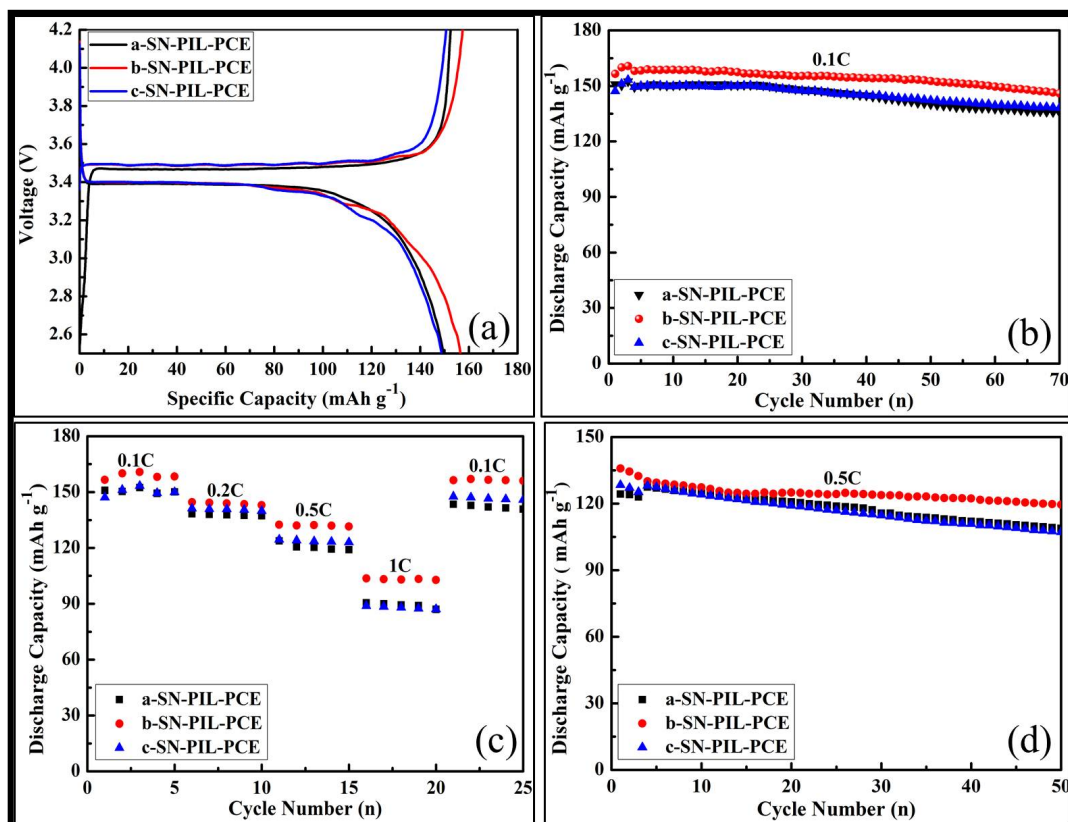


Fig. 7. First charge-discharge cycle curves of LiFePO₄/Li using a-PIL-SN-PCE, b-PIL-SN-PCE and c-PIL-SN-PCE as electrolytes at 0.1 C (a); Cycles capacities of LiFePO₄/Li assembled with a-PIL-SN-PCE, b-PIL-SN-PCE and c-PIL-SN-PCE electrolytes at 0.1 C (b); Rate performances of LiFePO₄/Li assembled with a-PIL-SN-PCE, b-PIL-SN-PCE and c-PIL-SN-PCE electrolytes at the current density from 0.1 C to 1 C (c); Full cells performances of LiFePO₄/LTO assembled with a-PIL-SN-PCE, b-PIL-SN-PCE and c-PIL-SN-PCE electrolytes at 0.5 C (d).

Fig. 7(a) shows the first charge-discharge profile of LiFePO₄/Li half cells in different PIL-SN-PCE electrolytes at 0.1 C at 25 °C. The half-cell in b-PIL-SN-PCE delivers the highest

reversible discharge capacity among the three samples, up to 156.5 mAh g⁻¹, whereas those in a-PIL-SN-PCE and c-PIL-SN-PCE deliver discharge capacities of 149.6 mAh g⁻¹ and 149.3 mAh g⁻¹, respectively. The higher capacity of the cell in b-PIL-SN-PCE is mainly attributed to its combination of excellent interfacial stability of sample toward electrodes and high ionic conductivity. Fig. 7(b) shows the cycling stability of half-cells in the three electrolytes at a current density of 0.1 C at 25 °C. The half-cell in b-PIL-SN-PCE exhibits a high discharge capacity and excellent capacity retention of 93.3% after 70 cycles, which can be attributed to the following two aspects. On the one hand, b-PIL-SN-PCE can mitigate the side reactions between the electrodes and the electrolyte by effectively trapping SN inside the PI matrix. On the other hand, b-PIL-SN-PCE has a relatively high ionic conductivity. Thus, b-PIL-SN-PCE exhibits a better balance between ionic conductivity and suppression of parasitic reactions of SN. This is further demonstrated in the Fig. 7(c) for the rate performances of the half-cells in the current density range of 0.1 C to 1 C. The discharge capacities of all the half-cells decrease with increasing current density. However, the half-cell in b-PIL-SN-PCE shows the best rate performances at different current densities. Particularly, at 1 C it delivers a discharge capacity close to 66% of that at 0.1 C. Furthermore, the full cell of LiFePO₄/b-PIL-SN-PCE/LTO as displayed in Fig. 7(d) shows an outstanding high initial discharge capacity of 132.4 mAh g⁻¹ at 0.5 C and an excellent capacity retention of 90.3% after 50 cycles. All above results suggest that b-PIL-SN-PCE is a promising candidate for application in LIBs.

4. Conclusion

In summary, PIL-SN-PCE electrolyte has been successfully synthesized by an in-situ method. It displays extraordinary thermal stability up to 300 °C, a remarkable electrochemical ability up to 5.4 V vs. Li/Li⁺, a high room temperature ionic conductivity of 6.54×10⁻⁴ S cm⁻¹. In addition, excellent interfacial compatibility between b-PIL-SN-PCE and electrodes ensure high rate performances and high capacity retention of both half cells and full cells, suggesting that it is promising solid state electrolyte for application in high energy LIBs.

Conflicts of interest:

There are no conflicts of interest to declare.

Acknowledgement:

This work was financially supported by the National Natural Science Foundation of China (No. 21476158, 21621004), Program for Chang jiang Scholars and Innovative Research Team in University (No. IRT_15R46). XG.S and S.D were supported by the U.S. Department of Energy, Office of Science, Basic Energy Sciences, Materials Sciences and Engineering Division. F. D and XJ. L were supported by the Foundation of National Key Laboratory of Science and Technology on Power Sources (No.9140C16020212-DZ2801), P. R. China.

References:

- [1] J. Alvarado, MA. Schroeder, TP. Pollard, X. Wang, JZ. Lee, M. Zhang, T. Wynn, M. Ding, O. Borodin, YS. Meng, K. Xu, Bisalt ether electrolytes: a pathway towards lithium metal batteries with Ni-rich cathodes, *Energy Environ. Sci.* 12 (2) (2019) 780-794.
- [2] SH. Lee, JY. Hwang, SJ. Park, GT. Park, YK. Sun, Adiponitrile (C₆H₈N₂): A New Bi - Functional Additive for High - Performance Li - Metal Batteries, *Adv. Funct. Mater.* 29 (30)

(2019) 1902496-1902505.

[3] Q. Zhao, X. Liu, S. Stalin, K. Khan, LA, Archer, Solid-state polymer electrolytes with in-built fast interfacial transport for secondary lithium batteries, *Nat. Energy* 4(5) (2019) 365-373.

[4] JF. Wu, X. Guo, Nanostructured Metal - Organic Framework (MOF)-Derived Solid Electrolytes Realizing Fast Lithium Ion Transportation Kinetics in Solid - State Batteries, *Small*. 15(5) (2019) 1804413-1804420.

[5] LN. Wu, J. Peng, YK. Sun, FM. Han, YF. Wen, CG. Shi, JJ. Fan, L. Huang, JT. Li, SG. Sun. A High-Energy Density Li metal Dual-Ion Battery with Lithium Nitrate-Modified Carbonate-Based Electrolyte, *ACS Appl. Mater. Interfaces* 11(20) (2019)18504-18510.

[6] SJ. Tan, J. Yue, XC. Hu, ZZ. Shen, WP. Wang, JY. Li, TT. Zuo, H. Duan, Y. Xiao, YX. Yin, R. Wen, Nitriding-Interface-Regulated Lithium Plating Enables Flame-Retardant Electrolytes for High-Voltage Lithium Metal Batteries, *Angew. Chem.* 131(23) (2019) 7884-7890.

[7] JY. Liang, XX. Zeng, XD. Zhang, TT. Zuo, M. Yan, YX. Yin, JL. Shi, XW. Wu, YG. Guo, LJ. Wan, Engineering Janus Interfaces of Ceramic Electrolyte via Distinct Functional Polymers for Stable High-Voltage Li-Metal Batteries, *J. Am. Chem. Soc.* 141 (23) (2019) 9165-9169.

[8] J. Zhang, J. Zhao, L. Yue, Q. Wang, J. Chai, Z. Liu, X. Zhou, L. Hong, Y. Guo, G. Cui Safety-reinforced poly(propylene carbonate)-based all-solid-state polymer electrolyte for ambient-temperature solid polymer lithium batteries, *Adv. Energy Mater.* 5 (24) (2015), Article 1501082

[9] L. Fan, S. Wei, S. Li, Q. Li, Y. Lu, Recent progress of the solid - state electrolytes for high - energy metal - based batteries. *Adv. Energy Mater.* 8 (11) (2018) 1702657-1702688.

- [10] L. Liu, X. Qi, S. Yin, Q. Zhang, X. Liu, L. Suo, H. Li, L. Chen, YS. Hu, In-Situ Formation of Stable Interface in Solid-State Batteries, *ACS Energy Letters*. 4 (7) (2019) 1650-1657.
- [11] Y. Ruan, Y. Lu, X. Huang, J. Su, C. Sun, J. Jin, Z. Wen, Acid Induced Conversion towards Robust and Lithiophilic Interface for Li-Li₇La₃Zr₂O₁₂ Solid-State Battery. *J. Mater. Chem. A*, 7 (2019) 14565-14574.
- [12] GT. Hitz, DW. McOwen, L. Zhang, Z. Ma, Z. Fu, Y. Wen, Y. Gong, J. Dai, TR. Hamann, L. Hu, ED. Wachsman, High-rate lithium cycling in a scalable trilayer Li-garnet-electrolyte architecture, *Mater. Today*, 22 (2019) 50-57.
- [13] X. Fan, X. Ji, F. Han, J. Yue, J. Chen, L. Chen, T. Deng, J. Jiang, C. Wang. Fluorinated solid electrolyte interphase enables highly reversible solid-state Li metal battery, *Sci. Adv.* 4 (12) (2018) 9245-9246.
- [14] C. Ma, K. Dai, H. Hou, X. Ji, L. Chen, DG. Ivey, W. Wei, High Ion-Conducting Solid-State Composite Electrolytes with Carbon Quantum Dot Nanofillers, *Adv. Sci.* 5(5) (2018) 1700996-1701006.
- [15] W. Yao, Q. Zhang, F. Qi, J. Zhang, K. Liu, J. Li, W. Chen, Y. Du, Y. Jin, Y. Liang, N. Liu, Epoxy containing solid polymer electrolyte for lithium ion battery, *Electrochim. Acta*. 318 (20) (2019) 302-313.
- [16] Y. Song, L. Yang, W. Zhao, Z. Wang, Y. Zhao, Z. Wang, Q. Zhao, H. Liu, F. Pan, Revealing the Short-Circuiting Mechanism of Garnet-Based Solid-State Electrolyte, *Adv. Energy Mater.* 9 (21) (2019) 1900671-1900677.
- [17] Y. Zhao, J. Yan, W. Cai, Y. Lai, J. Song, J. Yu, B. Ding, Elastic and well-aligned ceramic LLZO nanofiber based electrolytes for solid-state lithium batteries, *Energy Storage Mater.*

(2019).

[18] D. Liu, W. Zhu, Z. Feng, A. Guerfi, A. Vijnh, K. Zaghbi, Recent progress in sulfide-based solid electrolytes for Li-ion batteries, *Mater. Sci. Engineering: B*, 213 (2016) 169-76.

[19] RC. Xu, XH. Xia, ZJ. Yao, XL. Wang, CD. Gu, JP. Tu, Preparation of $\text{Li}_7\text{P}_3\text{S}_{11}$ glass-ceramic electrolyte by dissolution-evaporation method for all-solid-state lithium ion batteries, *Electrochim Acta*, 219 (2016) 235-240.

[20] F. Bertasi, G. Pagot, K. Vezzù, A. Nale, G. Pace, YH. Bang, G. Crivellaro, E. Negro, V. Di Noto, Lithiated Nanoparticles Doped with Ionic Liquids as Quasi-Solid Electrolytes for Lithium Batteries. *Electrochim Acta*. 307 (2019) 51-63.

[21] J. Shi, H. Xiong, Y. Yang, H. Shao, Nano-sized oxide filled composite PEO/PMMA/P(VDF-HFP) gel polymer electrolyte for rechargeable lithium and sodium batteries, *Solid State Ionics*, 326 (2018) 136-144.

[22] CL. Yang, ZH. Li, WJ. Li, HY. Liu, QZ. Xiao, GT. Lei, YH. Ding, Batwing-like polymer membrane consisting of PMMA-grafted electrospun PVdF-SiO₂ nanocomposite fibers for lithium-ion batteries, *J. Membr Sci.* 495 (2015) 341-350.

[23] X. Wang, X. Hao, Y. Xia, Y. Liang, X. Xia, J. Tu, A polyacrylonitrile (PAN)-based double-layer multifunctional gel polymer electrolyte for lithium-sulfur batteries, *J. Membr Sci.* 582 (2019) 37-47.

[24] LT. Khoon, NF. Zaini, NN. Mobarak, NH. Hassan, SA. Noor, S. Mamat, KS. Loh, KH. KuBulat, MS. Su'ait, A. Ahmad. PEO-based polymer electrolyte comprised of epoxidized natural rubber material (ENR50) for Li-Ion polymer battery application, *Electrochim Acta*. 316 (2019) 283-291.

- [25] S. Chen, F. Feng, Y. Yin, X. Lizo, Z. Ma, Plastic crystal polymer electrolytes containing boron based anion acceptors for room temperature all-solid-state sodium-ion batteries. *Energy Storage Mater.*, (2018).
- [26] K. Liu, F. Ding, J. Liu, Q. Zhang, X. Liu, J. Zhang, Q. Xu, A Cross-linking succinonitrile-based composite polymer electrolyte with uniformly dispersed vinyl-functionalized SiO₂ particles for Li-ion batteries. *ACS Appl Mater. Interfaces*, 8(36) (2016) 23668-23675.
- [27] HJ. Ha, EH. Kil, YH. Kwon, JY. Kim, CK. Lee, SY. Lee, UV-curable semi-interpenetrating polymer network-integrated, highly bendable plastic crystal composite electrolytes for shape-conformable all-solid-state lithium ion batteries, *Energy Environ Sci.* 5(4) (2012) 6491-6499.
- [28] Y. Lu, Y. Cai, Q. Zhang, L. Liu, Z. Niu, J. Chen, A compatible anode/succinonitrile-based electrolyte interface in all-solid-state Na-CO₂ batteries, *Chemical Sci.* 10 (15) (2019) 4306-4312.
- [29] Q. Zhang, K. Liu, F. Ding, W. Li, X. Liu, J. Zhang, Enhancing the high voltage interface compatibility of LiNi_{0.5}Co_{0.2}Mn_{0.3}O₂ in the succinonitrile-based electrolyte. *Electrochim Acta*, 298 (2019) 818-826.
- [30] MB. Effat, Z. Lu, A. Belotti, J. Yu, YQ. Lyu, F. Ciucci, Towards succinonitrile-based lithium metal batteries with long cycle life: The influence of fluoroethylene carbonate loading and the separator, *J. Power Sources.* 436 (2019) 226802.
- [31] N. Zhang, J. He, W. Han, Y. Wang, Composite solid electrolyte PEO/SN/LiAlO₂ for a solid-state lithium battery. *J. Mater. Sci.* 54 (13) (2019) 9603-9612.
- [32] D. Zhou, YB. He, R. Liu, M. Liu, H. Du, B. Li, Q. Cai, QH. Yang, F. Kang, In Situ

Synthesis of a Hierarchical All-Solid-State Electrolyte Based on Nitrile Materials for High-Performance Lithium-Ion Batteries, *Adv. Energy Mater.* 5 (15) 2015 1500353-1500364.

[33] P. Lv, J. Yang, G. Liu, H. Liu, S. Li, C. Tang, J. Mei, Y. Li, D. Hui, Flexible solid electrolyte based on UV cured polyurethane acrylate/succinonitrile-lithium salt composite compatibilized by tetrahydrofuran. *Composites Part B: Engineering.* 120 (2017) 35-41.

[34] K. Liu, F. Ding, Q. Lu, J. Liu, Q. Zhang, X. Liu, Q. Xu, A novel plastic crystal composite polymer electrolyte with excellent mechanical bendability and electrochemical performance for flexible lithium-ion batteries. *Solid State Ionics.* 289 (2016) 1-8.

[35] P. Lv, Y. Li, Y. Wu, G. Liu, H. Liu, S. Li, C. Tang, J. Mei, Y. Li, Robust Succinonitrile-Based Gel Polymer Electrolyte for Lithium-Ion Batteries Withstanding Mechanical Folding and High Temperature. *ACS Appl. Mater. Interfaces,* 10 (30) (2018) 25384-25392.

[36] Y. Lu, KW. He, SJ. Zhang, YX. Zhou, ZB. Wang, UV-curable-based plastic crystal polymer electrolyte for high-performance all-solid-state Li-ion batteries, *Ionics,* 25 (4) 2019 1607-1615.

[37] Y. Dong, T. Ding, LZ. Fan, A free-standing and thermostable polymer/plastic crystal electrolyte for all-solid-state lithium batteries, *Ionics,* 23 (12) 2017 3339-3345.

[38] QJ. Wang, HH. Fan, LZ. Fan, Q. Shi Preparation and performance of a non-ionic plastic crystal electrolyte with the addition of polymer for lithium ion batteries, 114 (2013) 720-725.

[39] YZ. Zheng, Y. Zhou, G. Deng, R. Guo, DF. Chen, Insight into the structure and interaction properties of 1-propylnitrile-3-methylimidazolium bis (trifluoromethylsulfonyl) imide and chloroform mixtures. *J. Molecular Liquids.* 283 (2019) 748-755.

[40] D. Zhang, L. Zhang, K. Yang, H. Wang, C. Yu, D. Xu, B. Xu, LM. Wang, Superior blends

solid polymer electrolyte with integrated hierarchical architectures for all-solid-state lithium-ion batteries. *ACS Appl. Mater. Interfaces*. 9 (42) (2017) 36886-36896.

[41] Y. Zhou, J. Hu, P. He, Y. Zhang, J. Xu, X. Wu. Corrosion suppression of aluminum metal by optimizing lithium salt concentration in solid-state imide salt-based polymer plastic crystal electrolyte membrane, *ACS Appl. Energy Mater.* 1(12) (2018) 7022-7027.

[42] SH. Kim, KH. Choi, SJ. Cho, J. Yoo, SS. Lee, SY. Lee, Flexible/shape-versatile, bipolar all-solid-state lithium-ion batteries prepared by multistage printing, *Energy Environ. Sci.* 11 (2) (2018) 321-30.

[43] Q. Wang, WL. Song, LZ. Fan, Q. Shi, Effect of alumina on triethylene glycol diacetate-2-propenoic acid butyl ester composite polymer electrolytes for flexible lithium ion batteries, *J. Power Sources*. 279 (2015) 405-412.

[44] H. Gao, L. Xue, S. Xin, K. Park, JB. Goodenough, A Plastic - Crystal Electrolyte Interphase for All-Solid-State Sodium Batteries. *Angew. Chem., Int. Ed.* 56 (20) (2017) 5541-5545.

[45] KH. CHoi, SH. Kim, HJ. Ha, EH. Kil, CK. Lee, SB. Lee, KS. J, SY. L, Compliant polymer network-mediated fabrication of a bendable plastic crystal polymer electrolyte for flexible lithium-ion batteries, *J. Mater. Chem. A*. 1 (2013) 5224-5233.

[46] KH. Choi, SJ. Cho, SH. Kim, YH. Kwon, JY. Kim, SY. Lee, Thin, Deformable, and Safety-Reinforced Plastic Crystal Polymer Electrolytes for High-Performance Flexible Lithium-Ion Batteries. *Adv. Funct. Mater.* 24 (1) (2014) 44-52.

[47] SH. Kim, KH. Choi, SJ. Cho, JS. Park, KY. Cho, CK. Lee, SB. Lee, JK. Shim, SY. Lee. A shape-deformable and thermally stable solid-state electrolyte based on a plastic crystal

composite polymer electrolyte for flexible/safer lithium-ion batteries. *J. Mater. Chem. A.* 2(28) (2014) 10854-10861.

[48] P.J. Alarco, Y. Abu-Lebdeh, A. Abouimrane, M. Armand, The plastic-crystalline phase of succinonitrile as a universal matrix for solid-state ionic conductors, *Nat. Mater.* 3(7) (2004) 476-481.

[49] Q.Q. Zhang, K. Liu, F. Ding, W. Li, X. Liu, J. Zhang, Safety-Reinforced Succinonitrile-Based Electrolyte with Interfacial Stability for High-Performance Lithium Batteries. *ACS Appl. Mater. Interfaces*, 9 (35) (2017) 29820-29828.

Supporting Information

In situ polymerized succinonitrile-based solid polymer electrolytes for lithium ion batteries

Kai Liu^{a,b,e}, Qingqing Zhang^a, Bishnu P Thapaliya^{b,e}, Xiaoguang Sun^b, Fei Ding^{c*}, Xingjiang Liu^{a,c}, Jinli Zhang^{a,d*}, Sheng Dai^{b,e}

^a School of Chemical Engineering and Technology, Tianjin University, Tianjin 300350, P. R. China.

^b Chemical Science Division, Oak Ridge National Laboratory, Oak Ridge, TN 37831, USA.

^c National Key Laboratory of Science and Technology on Power Sources, Tianjin Institute of Power Sources, Tianjin 300384, P. R. China.

^d School of Chemical Engineering, Shihezi University, Shihezi 832003, P. R. China.

^e Department of Chemistry, University of Tennessee, Knoxville, TN 37996, USA.

*Corresponding author's email address: feiding_ncps@163.com; zhangjinli@tju.edu.cn

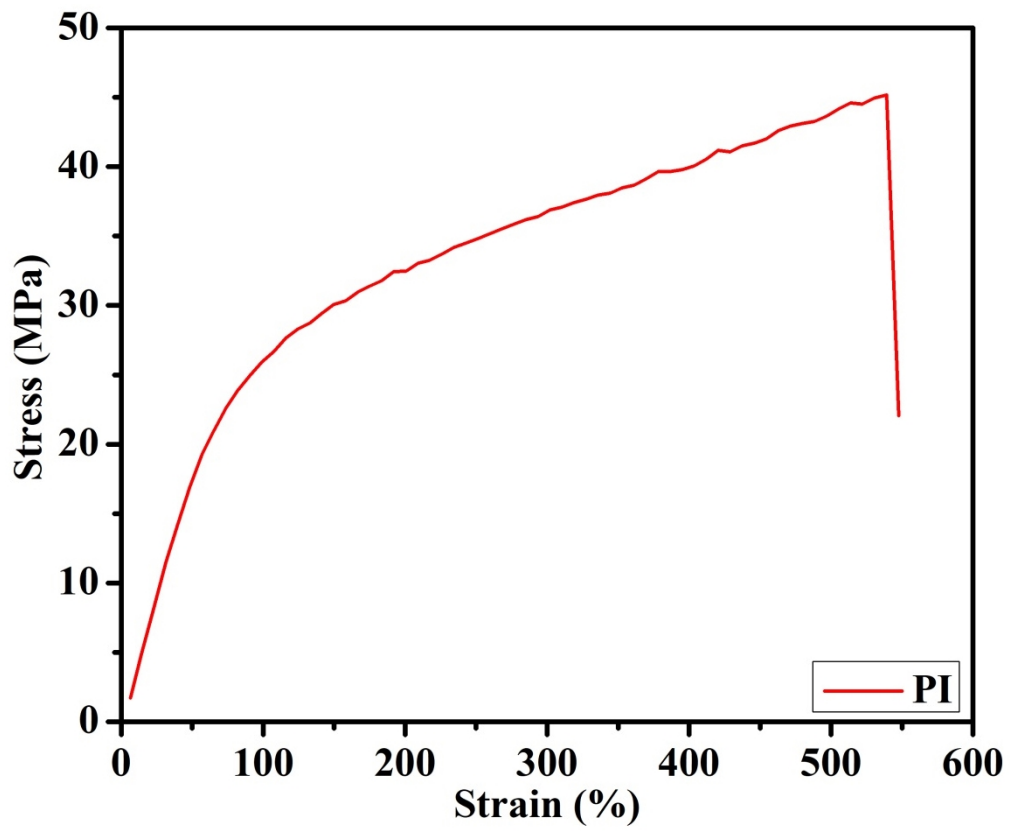


Fig. S 1. The stress-strain curve of PI

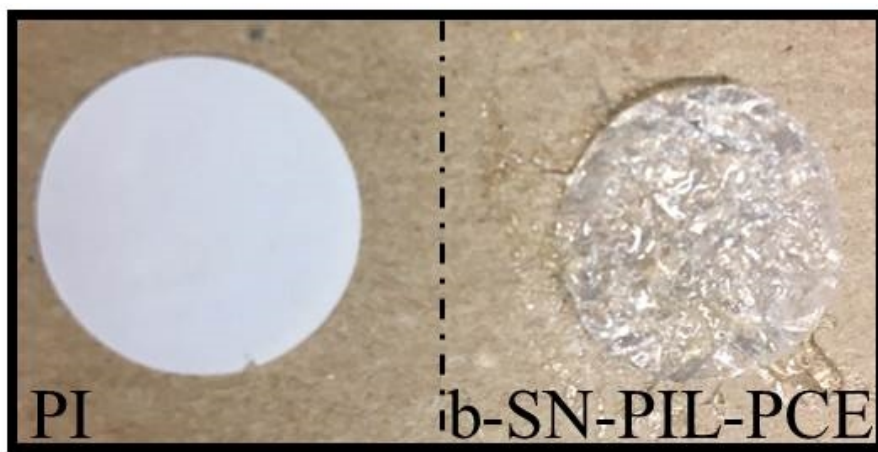


Fig. S 2. The optical photograph of pristine PI and b-SN-PIL-PCE

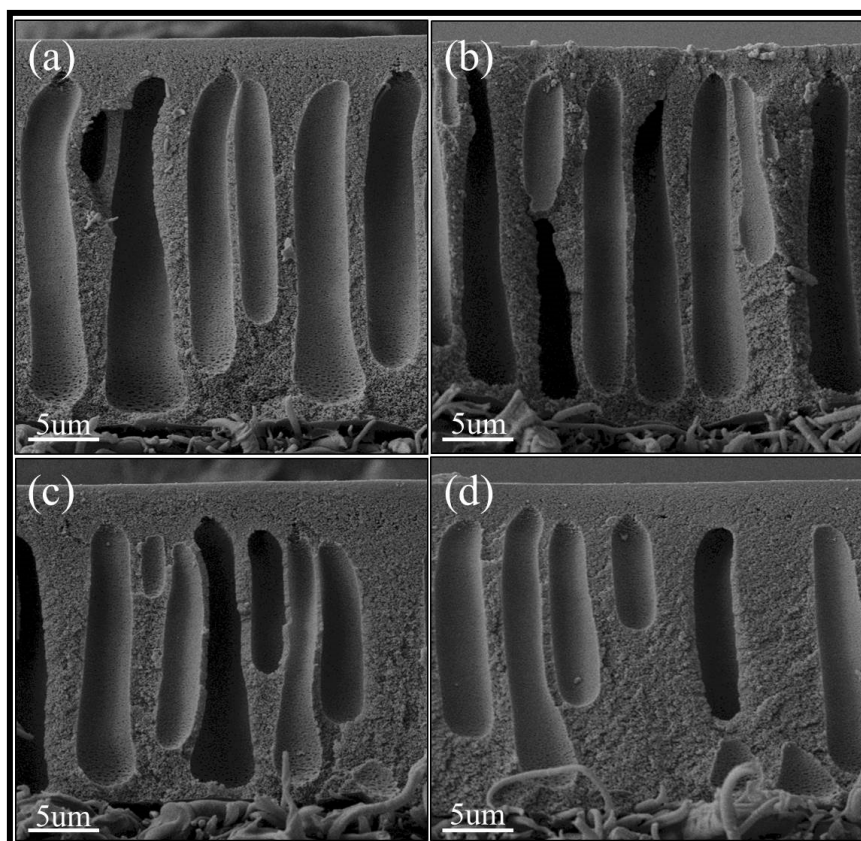


Fig. S 3. Whole cross-section morphological characteristics of pristine PI (a), polymerized PIL-SN-PCE electrolyte embedded into the PI supporting framework (b) a-PIL-SN-PCE, (c) b-PIL-SN-PCE, and (d) c-PIL-SN-PCE